PHYSICAL REVIEW A VOLUME 40, NUMBER 7 OCTOBER 1, 1989

# Contributions from ion-atom charge-exchange collisions to the C VI Lyman-series intensities in the Joint European Torus tokamak

M. Mattioli
*Association EURATOM–Commissariat à l'Energie Atomique sur la Fusion, Centre d'Etudes Nucléaires de Cadarache,*
*13108 Saint Paul lez Durance, France*

N. J. Peacock
*EURATOM–United Kingdom Atomic Energy Authority Fusion Association, The Culham Laboratory,*
*Abingdon, Oxon OX14 3DB, United Kingdom*

H. P. Summers and B. Denne
*Joint European Tokamak Joint Undertaking, Abingdon, Oxon OX14 3EA, United Kingdom*

N. C. Hawkes
*EURATOM–United Kingdom Atomic Energy Authority Fusion Association, The Culham Laboratory,*
*Abingdon, Oxon OX14 3DB, United Kingdom*

(Received 3 January 1989)

In a multiple-keV-temperature deuterium plasma such as that in the Joint European Torus (JET), C VI emission arises from excitation processes that, in the absence of neutral-hydrogen-beam heating, occur near the plasma boundary. Distortion to the C VI Lyman decrement, such as the Ly-$\beta$:Ly-$\gamma$:Ly-$\delta$ ratio, and enhancement of high series members (around 1$s$-12$p$) are observed. In this situation, large influxes of $D^0$ atoms are anticipated at the plasma boundary when the plasma is limited by the carbon inner wall. The intensities of the Lyman-series members are interpreted in terms of electronic excitation of $C^{5+}$ ions in their ground state as well as charge-exchange collisions between $C^{6+}$ ions and thermal $D^0$ atoms, either in their ground state or in their excited states (up to the collision limit). The line-of-sight emission is modeled using an impurity-ion transport code requiring knowledge of the electron temperature, electron density, and $D^0$ radial profiles. Comparison of the observed relative intensities of the C VI Lyman series Ly-$\beta$, Ly-$\gamma$, Ly-$\delta$, etc., with the model calculations allows plausible corrections to be made to the effective charge-exchange rate coefficients as a function of the principal quantum number. The observations offer a potential method of measuring local $D^0$ concentrations near the boundary in high-temperature, high-$D^0$-concentration recycling plasmas.

## I. INTRODUCTION

The influence of charge-exchange processes between impurity ions and neutral hydrogen isotopes has been reported in the observed line spectra from tokamak plasmas. These neutral hydrogen isotopes can be either thermal or beam neutral species. The atomic beams are used for heating or diagnostic purposes (or both) with energies in the tens of keV range. Background thermal neutral species are present in tokamak plasmas from the periphery to the center as a consequence of inward transport due to successive charge-exchange collisions with plasma ions. Their concentration is several orders of magnitude larger at the edge than at the center and several orders of magnitude lower than the electron density everywhere. Also secondary "halo" (produced by successive beam-plasma collisions) can add a substantial concentration of thermal charge-exchange neutral species at the center with atomic-beam heating. Such charge-exchange collisions also yield a supplementary recombination process for impurity ions and so influence impurity ionization equilibrium and impurity transport evaluations. The electrons "exchanged" between the neutral hydrogen isotopes and the impurity ions are predominantly captured into excited states of the recombined ions and so can be detected by observation of the cascade radiation emitted during decay to the ground state. From the decay spectral series, quantitative estimates of the ionic concentrations can be made, provided the effective charge-exchange rates (including cascades and level mixing) are reliable and the atomic densities and electron parameters in the plasma are known.

Generally, this allows detection of the fully stripped carbon and oxygen ions, not normally observable by line emission spectroscopy. Moreover, the impurity-ion temperature and toroidal rotation can be obtained by linewidth and line-shift evaluations. These techniques, called charge-exchange recombination spectroscopy, have been reviewed recently by Isler.[1] In the Joint European Torus (JET), measurements of the impurity-ion density, temperature, and rotation have been performed by observing visible transitions between highly excited levels of the recombined C and O H-like ions with the supplementary heating beams active.[2]

Space-resolved spectra of the $1s^2$-$1snp$ Ar XVII singlet lines have been observed in Alcator-C tokamak plasmas.[3,4] In these papers, in Ohmic plasmas without atomic beams the line intensity ratios could not be simulated by radiative cascades of the upper levels populated by electron collisions from the ground state, but charge-exchange collisions with thermal neutral species (either in their ground states or in their excited states) had to be added as a supplementary process populating the highly excited states. From a numerical simulation of the space-resolved spectra it was possible to obtain the neutral hydrogen radial density profile.

In this paper we shall present experimental carbon Lyman-series spectra obtained in ohmically heated and radio-frequency-heated JET plasmas. The uv spectrometers view the carbon inner wall directly along a horizontal chord. The outer belt limiters, being displaced from the horizontal, are not seen in this viewing geometry. When the plasma is brought into contact with the inner-wall [the so-called inner-wall (IW) plasmas to be distinguished from the limiter plasmas, in which the plasma current channel is limited by the outer belt limiters] modifications in the emission in the series extend to the series limit. The experimental C spectra then resemble both the previously mentioned Ar spectra[3,4] and the spectra predicted in Ref. 5 for the C and O Lyman series in presence of high-energy neutral beams.

In Sec. II, after a short description of the experimental setup, we shall present data from a 3.5-MA, 2.8-T JET discharge, which, having been initially started as a limiter discharge, is moved to the inner wall at about 5 sec after the beginning of the pulse. It is subsequently heated, between 11.5 and 15 sec, by 3 MW of radio-frequency (rf) power.

In Sec. III the impurity transport simulation code is described with particular attention to the atomic physics data, and then in Sec. IV the carbon Lyman spectra during three selected time intervals (corresponding to the three distinct experimental phases of the discharge) are simulated. In the simulations, the thermal deuterium neutral density $n_{\mathrm{D}}(r)$ radial profile is treated as a free adjustable parameter. To model all three experimental situations with "reasonable" $n_{\mathrm{D}}(r)$ profiles (i.e., not in contradiction to other diagnostics), it will be shown to be necessary to introduce corrective principal quantum number $(n)$-dependent multiplicative factors $F(n)$ for the effective charge-exchange rate coefficients for photon emission in the Lyman series.

In Sec. V, the possibility of measuring local $\mathrm{D}^0$ concentrations near the boundary of high-temperature, high-$\mathrm{D}^0$-concentration recycling plasmas is discussed.

## II. EXPERIMENT

### A. General

The 10–330 Å region is observed in JET by using the most recent version of the Schwob-Fraenkel 2-m grazing incidence extreme-ultraviolet (xuv) spectrometer.[6] It is located in the torus midplane and views the plasma along a central chord at a slight angle to the major radius of the JET torus. The spectral resolution (with a 600 grooves/mm grating) is 0.2 Å FWHM (full width at half maximum). The detector consists of two microchannel-plate (MCP) detectors movable along the Rowland circle. Each is associated with a phosphor screen image intensifier and coupled by a flexible fiber-optic conduit to a 1024-element photodiode array. In the present experiment, one detector is positioned to view the C VI-Lyman series, whereas the other includes in its spectral range the C VI 182.17-Å Balmer $\alpha$ line. Longer-wavelength carbon lines of lower ionizations (e.g., C III 977 Å and C IV 312.4 Å) are simultaneously observed with a McPherson vuv broadband survey spectrometer.[7] Absolute calibration is available only for the second spectrometer. Radial profiles of electron temperature $T_e(r)$, electron density $n_e(r)$, required for the simulation of the spectroscopic data, are obtained, respectively, from a LIDAR (light detection and ranging) Thomson scattering system[8] and

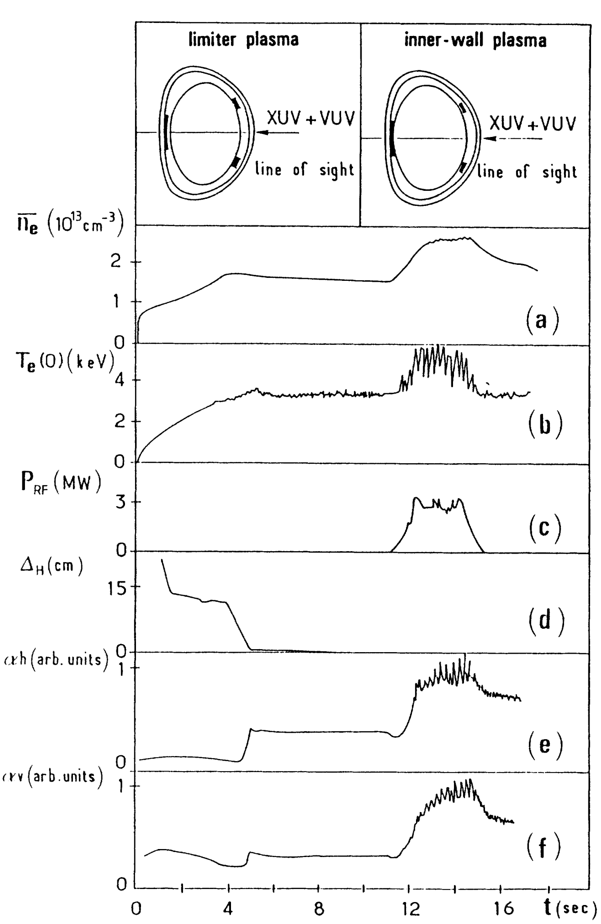

FIG. 1. Time evolution of a few signals for a JET discharge: (a) average line-integrated electron density $\bar{n}_e$ along a vertical chord through the plasma center, (b) central electron temperature $T_e(0)$, (c) rf power $P_{\mathrm{rf}}$, (d) plasma horizontal displacement $\Delta_H$ of the plasma border from the inner wall, (e) $\mathrm{D}_\alpha$ monitor signal viewing the inner wall horizontally $\mathrm{D}_{\alpha h}$, (f) vertical $\mathrm{D}_\alpha$ monitor signal $\mathrm{D}_{\alpha v}$. Top insets: schematic of the position of the last closed magnetic surface with respect to the inner wall and to the two outer belt limiters for limiter plasmas (left) and for IW plasmas (right).

from a FIR (far infrared radiation) laser interferometer[9] (in this case Abel inversion taking into account the shape of the magnetic surfaces is required).

### B. Discharges with large variations in the atomic deuterium influxes

In the following, a representative discharge showing changes in the C VI Lyman-series intensities is analyzed. The discharge chosen is one of a series of deuterium discharges with plasma current $I_p = 3.5$ MA, toroidal magnetic field $B_T = 2.8$ T, $^3$He prefilling, and a few percent of H addition for ion-cyclotron rf minority heating.

Time-resolved signals showing the discharge evolution are presented in Fig. 1 as follows: the average line-integrated electron density $\bar{n}_e(t)$, the maximum central electron temperature $T_e(0,t)$ from electron cyclotron emission, the rf power, the horizontal distance $\Delta_H$ between the plasma and the inner wall, and two $D_\alpha$ (Deuterium Balmer-$\alpha$ line) monitors. The upper $D_\alpha$ signal in Fig. 1, $D_{\alpha h}$, views horizontally both the plasma column

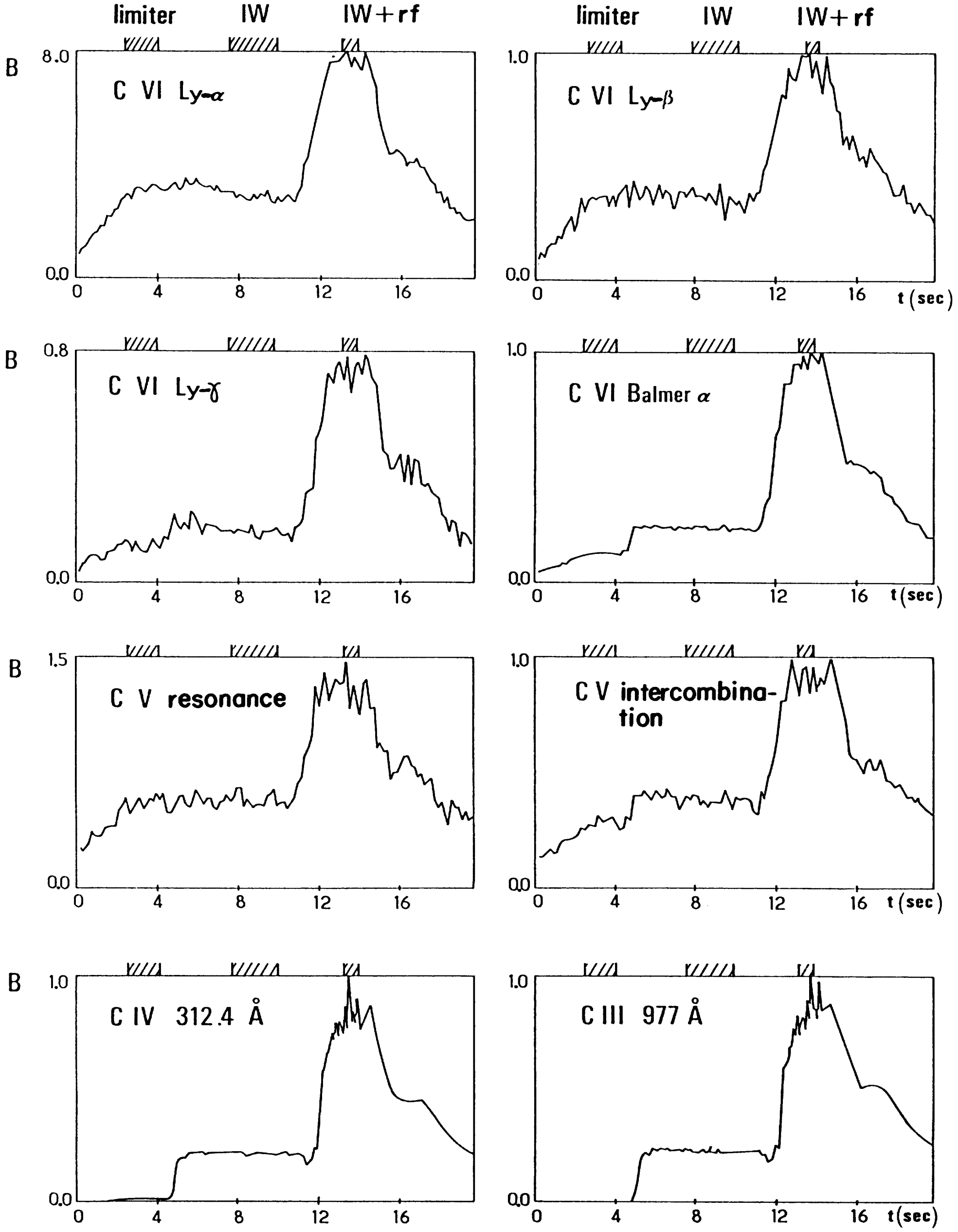

FIG. 2. Time evolution of the brightnesses $B$ of the following carbon lines: C VI Ly-$\alpha$, -$\beta$, and -$\gamma$; C VI Balmer-$\alpha$; C V resonance and intercombination; C IV 312.4 Å; and C III 977 Å. The three hatched time intervals correspond to the times over which the Lyman-series spectra shown in Figs. 3–5 were averaged.

and the inner wall, while the lower $D_{\alpha v}$ observes the plasma vertically far from limiters and rf antennae.

The discharge starts as a limiter discharge ($\Delta_H \sim 12$ cm and low $D_{\alpha h}$ signal). After 5 sec the plasma is moved towards the inner wall ($\Delta_H \sim 0$, with concomitant large $D_{\alpha h}$ signals and with $D_{\alpha v}$ signals practically unchanged). After an almost steady-state phase lasting until ~11.5 sec, 3 MW of rf power are applied between 11.5 and 15 sec during which there are increased values of both $n_e$ and $T_e$. The discharge remains on the inner wall throughout the additional heating. In the upper insets of Fig. 1 a schematic of the two plasma configurations is given, showing the last closed surface in contact either with the inner wall (right, IW plasma) or with the belt limiters (left, limiter plasma). The lines of sight of both the extreme ultraviolet spectrometer and the vacuum ultraviolet (vuv) spectrometer are also shown.

In Fig. 2 the time evolutions of a number of relevant spectroscopic signals are shown (namely, C VI Ly-$\alpha$, Ly-$\beta$, and Ly-$\gamma$, C VI Balmer-$\alpha$, the C V resonance and intercombination lines, as well as C IV 312.4 Å and C III 977-Å lines). For lines sufficiently near in wavelength (C VI Ly-$\alpha$, Ly-$\beta$, and Ly-$\gamma$, C V resonance and intercombination) relative ordinate scales are given in order to deduce intensity ratios. All the line brightnesses increase during the rf heating period (the same being true for the two $D_\alpha$ signals presented in Fig. 1). By contrast, at the limiter-inner-wall movement the brightness time evolutions depend on the individual lines. C VI Ly-$\alpha$ and Ly-$\beta$ along with C V resonance are not much affected by the plasma displacement, whereas all the other brightnesses show some degree of discontinuity by as much as ~30% for the C V intercombination line, ~40% for the C VI Ly-$\gamma$ line, ~100% for the C VI Balmer-$\alpha$ line, and by one order of magnitude or more for the two C lines of lower ionization. With IW plasmas, since the carbon sources are viewed directly (see Fig. 1 inset), the C III and C IV brightnesses represent the local carbon influx rather than the influx averaged over the entire plasma surface.[10]

### C. C VI Lyman-series spectra

The multichannel spectrometer records the entire C VI Lyman spectrum. Three spectra showing the region from

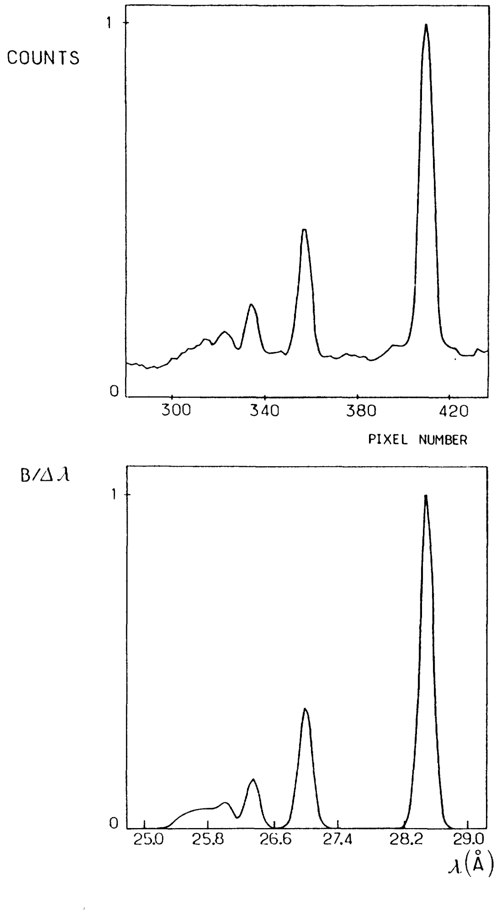

FIG. 3. Upper: experimental limiter plasmas Lyman-series spectrum integrated between 2.5 and 4.2 sec, the count number $C$, normalized to its maximum value at the Ly-$\beta$ wavelength, is given as function of the pixel number. Lower: simulated spectrum using curve 2 of Fig. 7(a) for $n_D(r)$. The calculated brightness per unit wavelength $B/\Delta\lambda$ is plotted as function of the wavelength. The normalization is same as for upper figure.

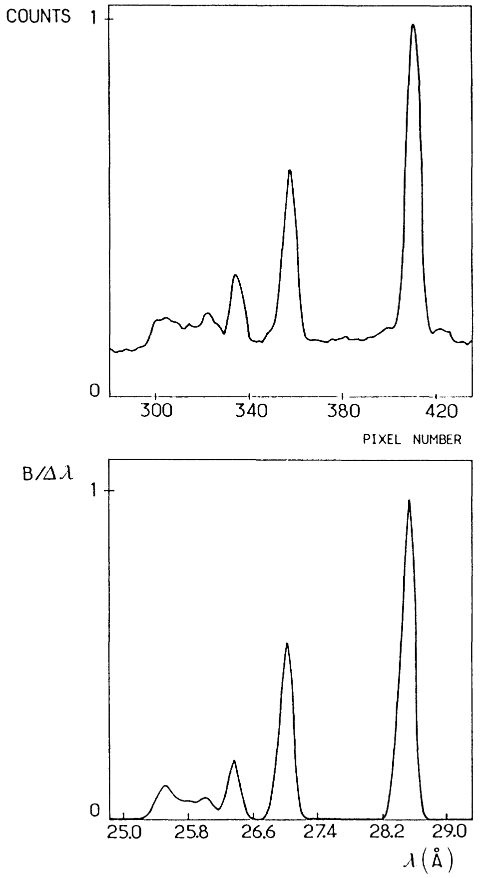

FIG. 4. Same as Fig. 3 for Ohmic IW plasmas with the experimental spectrum integrated between 7.7 and 10.0 sec. The simulated spectrum is obtained using curve 2 of Fig. 7(b) for $n_D(r)$.

Ly-$\beta$ up to the series limit are presented in Figs. 3 to 5 (upper), corresponding to the three phases of interest in the discharge. The corresponding time intervals are shown hatched in Fig. 2. In contrast to the spectrum of the limiter plasma in Fig. 3, in which the intensities of successive Lyman lines decrease monotonically with increasing quantum number $n$ of the upper level, the spectra presented in Figs. 4 and 5 show reduced Ly-$\beta$:Ly-$\gamma$ and Ly-$\beta$:Ly-$\delta$ ratios and enhanced emission up to the series limit. Due to the 0.2-Å FWHM resolution, lines above Ly-$\epsilon$ are not resolved individually. This enhanced emission manifests itself as a "bump," the peak of which corresponds to about the $1s$-$12p$ member. It should be noted that similar modifications of line intensity ratios have been seen also in the $1s^2$-$1snp$ singlet He-like C ion spectra.[11,12] For IW plasmas, enhancement of the C V series emission (albeit without the bump) was observed up to the series limit. The He-like ion spectra will not be analyzed qualitatively in this paper, since the available charge-exchange cross-section data leading to recombined He-like ions are not as well known as those leading to recombined H-like ions.

The spectra shown in Figs. 3 and 5 (upper) give the detected signals (count number) as function of the wavelength (pixel number). The experimental count numbers have been corrected for pixel gain fatigue. The problem was first recognized on displacing the detector carriage around the Rowland circle, when "holes" appear in background signal levels at the pixels corresponding to the previous positions of the strongest lines. Pixel to pixel gain variations can arise due to differential aging of the MCP.[13] The raw count numbers have been corrected by measuring the response to a continuum source provided by the plasma itself during a cold disruptive phase. The effect of these corrections is to increase the strong lines with respect to the weaker ones. They are most serious for the most intense lines such as Ly-$\alpha$ and have also been included in the ordinate scales of Fig. 2.

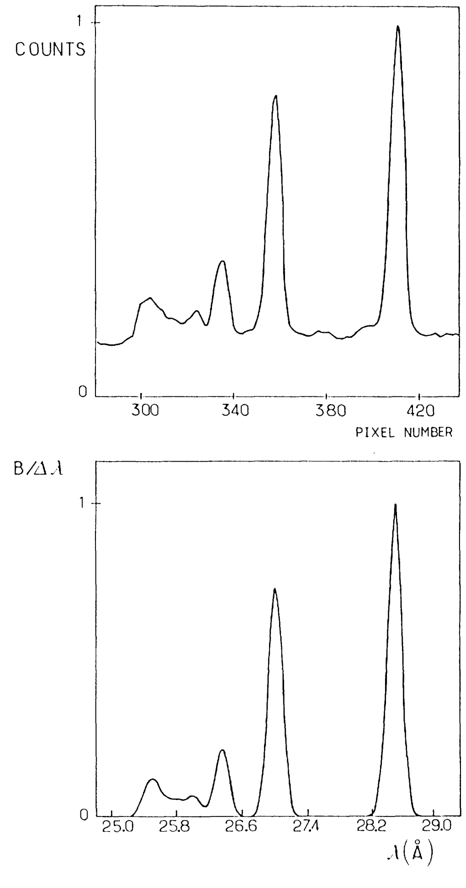

FIG. 5. Same as Fig. 3 for rf-heated IW plasmas with the experimental spectrum integrated between 13.2 and 14.0 sec. The simulated spectrum is obtained using curve 3 of Fig. 7(b) for $n_D(r)$.

## III. IMPURITY TRANSPORT SIMULATION CODE

### A. Description of the code

Impurity transport in tokamak plasmas is studied by solving for each atomic species the following impurity transport system in cylindrical geometry:

$$\frac{\partial n_Z}{\partial t}=-\frac{1}{r}\left[\frac{\partial}{\partial r}(r\Gamma_Z)\right]+n_e(n_{Z-1}S_{Z-1}-n_ZS_Z+n_{Z+1}\alpha_{Z+1}^{R}-n_Z\alpha_Z^{R})+n_D(n_{Z+1}\alpha_{Z+1}^{CE}-n_Z\alpha_Z^{CE})-\frac{n_z}{\tau_p}\,, \quad Z=1,\ldots,Z_N \qquad (1)$$

where $\Gamma_Z$ is the radial particle flux density (positive when directed outwards) of the ions of charge $Z$ of an element of nuclear charge $Z_N$. $n_Z$ is the corresponding ion density. $S_Z$, $\alpha_Z^R$, and $\alpha_Z^{CE}$ are, respectively, for the ions of charge $Z$ the ionization rate coefficients, the radiative plus dielectronic recombination rate coefficients, and the charge-exchange recombination rate coefficients. $\tau_p$ [different from infinity only in the scrape-off layer (SOL)] is the impurity confinement time for particle transport along the field lines.

Input parameters of the code are the $n_e(r)$ and $T_e(r)$ profiles along with the thermal neutral deuterium radial profile $n_D(r)$. $S_Z$, $\alpha_Z^R$, and $\alpha_Z^{CE}$ are functions of the radius $r$ because of their electron temperature dependence. In the evaluation of $\alpha_Z^{CE}$ it is supposed that both the recombining C ions and the $D^+$ ions have the same temperature $T_i$ as the neutral deuterium atoms $T_D$ and that this temperature can be taken equal to $T_e$, at least in the external plasma region. Note that deuterium is the JET filling gas.

A separate equation has to be included to describe the ionization of neutral carbon of density $n_0$. The boundary condition at the last mesh radius $r=a$ is written as

$$\Gamma_0(a)=n_0(a)V_0=R\sum_Z\Gamma_Z(a)+\Gamma_{\text{ext}}\,, \qquad (2)$$

that is, $\Gamma_0(a)$, the total neutral carbon flux density entering into the plasma with directed velocity $V_0$, is set equal to the sum of an external flux density $\Gamma_{\mathrm{ext}}$ and a recycling flux density. The latter is the total outward flux density $\sum_Z \Gamma_Z(a)$ at the last mesh recycled with recycling coefficient $R$. The radial flux density $\Gamma_Z$ is described by the following expression:

$$\Gamma_Z = -D_A \frac{\partial n_Z}{\partial r} - \frac{r}{a} V_A n_Z \ , \tag{3}$$

where $D_A$ (diffusion coefficient) and $V_A$ (inward convention velocity) are two transport parameters independent of $Z$ and of $r$.

The numerical solution of system (1) is the same as used previously for TFR plasma simulations[14] and is based on the procedure described in Ref. 15.

### B. Atomic physics data

The atomic subroutines on ionization balance are regularly updated to include the most recent theoretical collision data. For carbon ions, in the present version of the code, the ionization rate coefficients $S_Z$ are taken from the Queen's University of Belfast assessments[16] (updated in Ref. 17 for Li-like ions). The recombination rate coefficients $\alpha_Z^R$ are obtained as described in Ref. 18, while the total charge-exchange recombination rate coefficients $\alpha_Z^{\mathrm{CE}}$ are taken from the recent ORNL assessments.[19]

Line brightnesses and emissivities are also predicted, generally in the coronal population approximation. The atomic physics data utilized can be found in Ref. 20. Here it is sufficient to recall that the two He-like ion lines (C V resonance and intercombination lines) cannot be evaluated in the coronal population approximation. The calculations of Ref. 21 have been updated[20] to evaluate the intensity ratio of these two lines (the so-called $G$ ratio well known by astrophysicists). Charge-exchange contributions need to be included in the code by supposing that three quarters of the recombining collisions (i.e., $0.75\alpha^{\mathrm{CE}}$ for $\mathrm{C}^{5+}$ recombination) populate excited triplet states and that deexcitation to the ground state is only possible through the intercombination line. This is a relatively crude approximation.

### C. Line emission from H-like carbon ions

To simulate H-like C ion emission a more sophisticated model has been adopted, since not only electron excitation from the ground-state and charge-exchange collisions with deuterium atoms (both in ground and excited states) contribute, but redistribution and cascades modify their effects. The emission is modeled in a $nlj$ subshell resolved calculation including principal quantum shells $n$ up to 20.[2,22] The model gives effective excitation rate coefficients for photon emission in all the Lyman- and Balmer-series lines decomposed into electron-impact parts $Q_{n-1}^e$, $Q_{n-2}^e$, and charge-exchange parts $Q_{n-1}^{\mathrm{CE}}$, $Q_{n-2}^{\mathrm{CE}}$. It is to be noted that the corresponding contributions to the emissivities are, respectively, proportional to $n_e n_{\mathrm{C}^{5+}}$ and to $n_{\mathrm{D}} n_{\mathrm{C}^{6+}}$. Local electron, ion, and neutral deuterium temperatures and densities are used consistent with the ionization stage transport model.

An extension of the original model for the charge-exchange effective rates was required to allow proper treatment of high-series members. Charge transfer from thermal neutral hydrogen isotopes in the $1s$ state to form excited states of $\mathrm{C}^{5+}$ is strongly selective into principal quantum shell $n_{\mathrm{crit}}(1s)$ of the receiving ion with very small contributions to levels $n > n_{\mathrm{crit}}(1s)$. The $1s$ in parentheses describes the state of the hydrogen isotopes. $n_{\mathrm{crit}}(1s)$ ($\sim 4$ for C) is the level for which the charge-exchange cross section is a maximum. The cross sections for electron transfer from excited principal quantum shells $n_h$ of hydrogen isotopes scale approximately as $n_h^4$, while the associated $n_{\mathrm{crit}}(n_h)$ scales as $n_h n_{\mathrm{crit}}(1s)$. Excited states of the donor atom are therefore the principal source for populating the very high-$n$ $\mathrm{C}^{5+}$ shells. Relevant excited hydrogen isotope levels are restricted to $n_h \leq 5$ (the collision limit). The collision limit for $\mathrm{C}^{5+}$ is $\geq 20$ in the present conditions and it does not influence the calculations. A collisional-radiative model has been

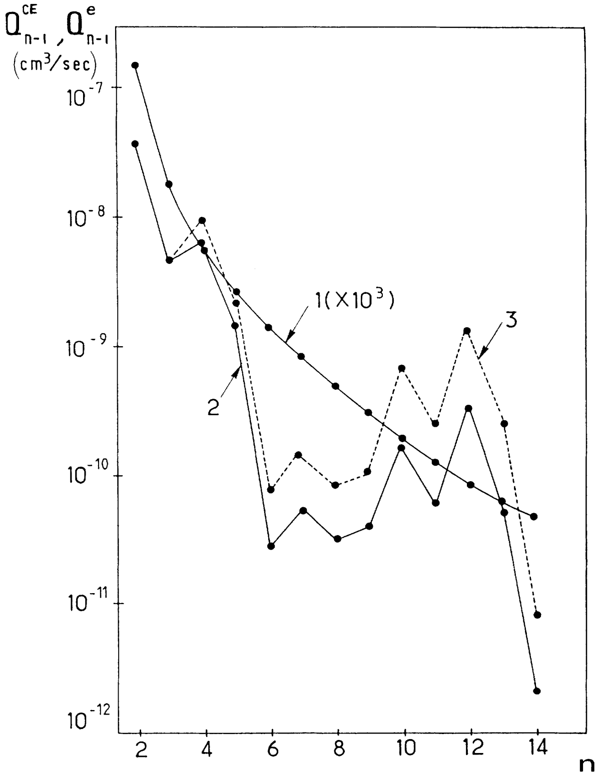

FIG. 6. Effective excitation rate coefficients for photon emission of Lyman-series lines as a function of the principal quantum number $n$ of the upper level. Curve 1 (solid): rate coefficients for electron impact from ground state $Q_{n-1}^e$ ($\times 10^3$), curve 2 (solid): rate coefficients for charge exchange with deuterium atoms $Q_{n-1}^{\mathrm{CE}}$, curve 3 (dashed): "corrected" rates $F(n)$ $Q_{n-1}^{\mathrm{CE}}$, after multiplication by an $n$-dependent multiplicative factor $F(n)$ [$F(4,5)=1.5$, $F(6-9)=2.5$, $F(10-14)=4$]. The rates shown are calculated for plasma parameters close to the region of maximum C VI line emission as follows: $n_e = 1.4\times 10^{13}$ cm$^{-3}$, $T_e \sim 500$ eV, $T_i = T_{\mathrm{D}} = T_e$, $Z_{\mathrm{eff}} = 2$.

used in the "bundle-$n$" picture[22] to calculate the excited level population of deuterium up to the collision limit.

Low-energy $n$-shell selective charge transfer cross sections from D(1$s$) have been taken from close-coupling molecular orbital (CCMO) calculations.[23] There are little data available for capture cross sections from excited states of thermal neutral hydrogen isotopes. As a basis for comparison with experiments, we have adopted the Landau-Zener (LZ) approximation based on the generalized $H_{12}^{*}$ coupling matrix element from Ref. 24. An over-barrier model[25] gives larger values (by factors $\sim 4-5$) and with higher $n_{\mathrm{crit}}(n_h)$. The expectation[24] is that the true values should lie between these two approximations. It is assumed that the capture is strongly selective into the appropriate $n_{\mathrm{crit}}$ and the $l$ distribution is as for capture from ground-state atoms. The latter is not critical for calculating the $l$-state redistribution.

The solid curves in Fig. 6 show as a function of the quantum number $n$ the theoretical effective electron-impact and charge-exchange rate coefficients ($Q_{n-1}^{e}$ and $Q_{n-1}^{\mathrm{CE}}$) for the Lyman series. The plasma parameters $T_e \sim 500$ eV, $T_i = T_e = T_{\mathrm{D}}$, $n_e \sim 1.4\times 10^{13}$ cm$^{-3}$, $Z_{\mathrm{eff}} \sim 2$, chosen for these calculations approximate to those which obtain in the region of dominant C VI emission. The detailed confrontation of experiment and theory to be described in Sec. IV indicates that the $Q_{n-1}^{\mathrm{CE}}$ rates, especially those associated with capture from neutral excited states, should be increased, by multiplying them by an $n$-dependent factor $F(n)$ ($\times 1.5$ for $n=4,5, \times 2.5$ for $n=6-9$, and $\times 4$ for $n=10-15$). The "corrected" $Q_{n-1}^{\mathrm{CE}}$ are shown by the dashed line and will be discussed further in the conclusions.

## IV. NUMERICAL SIMULATIONS OF THE CARBON LYMAN-SERIES SPECTRA

### A. General considerations

The $n_e(r)$ and $T_e(r)$ profiles required for the analysis are obtained by symmetrizing about the center of the last closed magnetic surface the full profiles across the whole plasma diameter (on the horizontal plane along the torus major radius). In this way both the inward displacement and the increased plasma dimension of the IW plasmas may be incorporated. The profiles are extrapolated up to the last mesh radius $a$. This is set a few centimeters beyond the limiter radius $a_L$ of the last closed magnetic surface. Decay lengths comparable to those given by Langmuir probes in similar plasma conditions are adopted in the extrapolation. For the three plasma conditions simulated by the code, Table I gives the values of $T_e$ and $n_e$ at the center, at the radius $a_c$ of maximum simulated C VI line emissivity, and at the limiter radius $a_L$. The deuterium neutral density profile $n_{\mathrm{D}}(r)$ has been treated in the code as an adjustable parameter which can be varied to match the simulated and experimental spectra. From the three neutral particle analyzers (NPA) (Ref. 26) it is possible to obtain the maximum deuterium ion temperatures along the lines of sight. The D$^0$ concentration profiles are inferred[26] from analysis of the energy spectra of the neutral particles emitted from JET. Note that the analyzed particles come from a radial extent up to $\sim(\frac{1}{2}-\frac{2}{3})\, a_L$ and that the deduced profiles are globally consistent with NPA measured fluxes. However, the numerical values, especially at larger radii up to the limiter radius $a_L$, have to be considered as tentative, since these are based only on a numerical neutral-particle transport code.

We use as our starting point for $n_{\mathrm{D}}(r)$ for limiter plasmas and for IW plasmas (both ohmic and rf heated) the two solid line curves of Fig. 7. The limiter plasma curve [(a), curve 1] is a lower limit from NPA simulations of JET limiter plasmas, whereas for IW plasmas the reference curve [(b), curve 3] is quite near to the curve given by NPA simulations of similar IW ohmic plasma conditions. The dashed curves are obtained by keeping constant $n_{\mathrm{D}}$ values in the central region and increasing or decreasing $n_{\mathrm{D}}$ values in the peripheral plasma with respect to the reference curves.

Numerically the two transport parameters (see formula 3) are taken as $D_A = 10^4$ cm$^2$/sec and $V_A = 200$ cm/s. The effect of varying them [within ranges believed typical for JET (Refs. 27 and 28)] will be discussed at the end of Sec. IV C.

Other parameters required for the simulations are the impurity confinement time $\tau_p$ in the SOL (between $a$ and $a_L$), the recycling coefficient $R$, the velocity $V_0$, and the external flux density $\Gamma_{\mathrm{ext}}$ of the incoming C atoms. Numerically, we choose $\tau_p = 10$ msec, $R=0$, $V_0 = 4\times 10^5$ cm/s. A steady-state solution for constant $\Gamma_{\mathrm{ext}}$ of arbitrary magnitude is sought, which could then be normalized by comparison with absolute line brightnesses.

### B. Radial ion distribution

The ion density radial profiles for IW plasmas are shown in Fig. 8 (upper) for three $n_{\mathrm{D}}$ profiles, (a) without

TABLE I. Electron temperatures and electron densities adopted in the code for the simulation of the three experimental spectra shown in Figs. 3–5 (upper). The values at the center, at the radius $a_c$ of maximum simulated C VI line emissivity [the simulated spectra being given in Figs. 3–5 (lower)], and at the limiter radius $a_L$ are given.

| | | Center | | | Peak emission | | | Limiter | |
|---|---|---|---|---|---|---|---|---|---|
| Plasma | $r=0$ | $T_e$ (keV) | $n_e$ ($10^{13}$ cm$^{-3}$) | $r=a_c$ (cm) | $T_e$ (keV) | $n_e$ ($10^{13}$ cm$^{-3}$) | $r=a_L$ (cm) | $T_e$ (keV) | $n_e$ ($10^{13}$ cm$^{-3}$) |
| Limiter | 0 | 2.9 | 2.25 | 96 | 0.28 | 1.25 | 112 | 0.08 | 0.15 |
| Inner wall | 0 | 2.9 | 2.45 | 96 | 0.30 | 1.35 | 118 | 0.075 | 0.22 |
| rf-heated IW | 0 | 4.4 | 3.4 | 98 | 0.60 | 2.2 | 120 | 0.15 | 0.25 |

neutral particles, and (b) and (c) with neutral-particle density profiles from curves (2) and (3) of Fig. 7(b), respectively. In the same Fig. 8 (lower), the emissivities of representative lines of C III, C IV, C V, and C VI are shown. The figure caption indicates the scale factors by which both the ion densities, normalized to the central total ion density, and the line emissivities, normalized to the C III 977-Å maximum emissivity for case (a) have been multiplied.

It appears that varying the $n_D(r)$ curve, while keeping other parameters constant, has a large effect on the line radiances. For example, between the two limiting situations shown in Fig. 8, the C VI Ly-$\beta$, C V resonance, C IV 312.4- and C III 977 Å brightnesses vary, respectively, by factors of 4.5, 6.5, 30, and 7. This fact is associated with the much slower effective ionization of carbon ions when charge-exchange processes are present. It is apparent in Fig. 8 since, progressing from (a) to (c), the $C^{3+}$ to $C^{5+}$ ion densities increase and the emissivity shells are displaced inwards. The brightness increase is an important point which will be considered further in Sec. IV D. It will be proved that $n_D$ increases significantly after moving to IW, and then a contradiction appears between the brightness dependence on $n_D$ and the fact that (see Fig. 2) C VI Ly-$\alpha$ and Ly-$\beta$ and C V resonance lines are practically constant at the limiter–inner-wall shift.

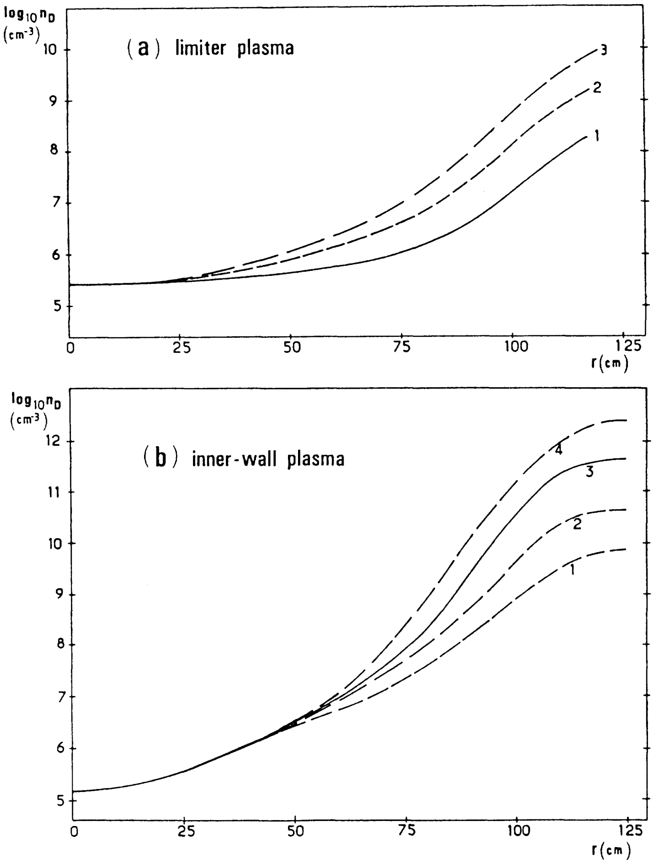

FIG. 7. Logarithm of the thermal neutral deuterium density profiles $n_D(r)$ adopted in the impurity transport simulation code. (a) Limiter plasmas, (b) IW plasmas. The solid curves show the initial profiles, suggested by NPA data. The dashed curves show the other profiles used for the simulations. The limiter radii $a_L$ are given in Table I; the last mesh radii $a$ are about 5 cm larger than $a_L$.

### C. Simulations of experimentally observed Lyman spectra

Once the steady-state solution of Eq. (1) is attained, a subroutine plots the simulated Lyman spectra from the calculated brightnesses assuming a Gaussian instrumental function of 0.2 Å FWHM. The line brightnesses per unit wavelength are plotted in arbitrary units, as a function of the wavelength $\lambda$ (in Å) from Ly-$\beta$ up to the 1$s$-15$p$ line. The instrumental resolution allows the distinct lines to be obtained up to Ly-$\epsilon$, whereas individual higher $n$ lines are not resolved. The "apparent" emission reaching the series limit at 25.3 Å. Examples of simulated spectra to be discussed in the following are shown in Figs. 3 and 5 (lower).

From preliminary simulations described in Ref. 20 it was concluded that the theoretical effective charge-exchange rates $Q_{n-1}^{\mathrm{CE}}$ had to be multiplied by an $n$-dependent factor $F(n)$ larger than one. The chosen values [$F(n)=1.5$ for $n=4,5$, $=2.5$ for $n=6$–9, and $=4$ for $n=10$–15] were necessary to simulate the reduced Ly-$\beta$:Ly-$\gamma$ and Ly-$\beta$:Ly-$\delta$ ratios and the large-$n$ bump associated with inner-wall plasmas.

Clearly, the estimated $n_D(r)$ curve is affected by the $F(n)$ values [the larger $F(n)$ the smaller the inferred deuterium densities] and, moreover, the low-$n$ $F(n)$ multiplicative factors must not be increased by greater than a factor of 2 at most to remain consistent with the total charge-exchange rate for $C^{6+}$ $\alpha^{\mathrm{CE}}$ which is believed to be reliable.

A first constraint for the final choice of $F(n)$ was the fact that curve (4) of Fig. 7(b) had to be considered as an upper limit, since larger $n_D$ values have never been inferred in JET either from NPA data analysis or from $D_\alpha$ monitors. A second constraint can be obtained from the quantitative analysis of the $D_\alpha$ monitor signals during the limiter phase. Simple considerations from the absolute brightnesses shown in Fig. 1[(e) and (f)] give peripheral $n_D$ values of a few $10^9$ cm$^{-3}$. The excited-state populations are taken from Ref. 29. The assumption of poloidal symmetry of $D_\alpha$ emission is justified by the similar brightnesses on the two $D_\alpha$ monitors observing the plasma vertically and horizontally. A SOL thickness of ~5 cm is assumed with comparable atomic and molecular neutral-particle production at the boundary. Since no large-$n$ bump and high Ly-$\beta$:Ly-$\gamma$ ratios appear on the corresponding spectra [see Fig. 3 (upper)], the $F(n)$ multiplicative factors must not be so large that they produce such a bump nor give too low Ly-$\beta$:Ly-$\gamma$ ratios when $n_D(a)$ is of the order of $(1.5-3)\times10^9$ cm$^{-3}$.

Table II shows the experimental and simulated Ly-$\beta$:Ly-$\gamma$ and Ly-$\beta$:Ly-$\delta$ ratios for the three separate phases of the discharges. Column $C$ indicates the $n_D$ curve number from Fig. 7 [(a) for limiter plasmas, (b) for both IW plasmas]. The final quantitative comparison is based on the Ly-$\beta$:Ly-$\gamma$ ratio (rather than on the much less

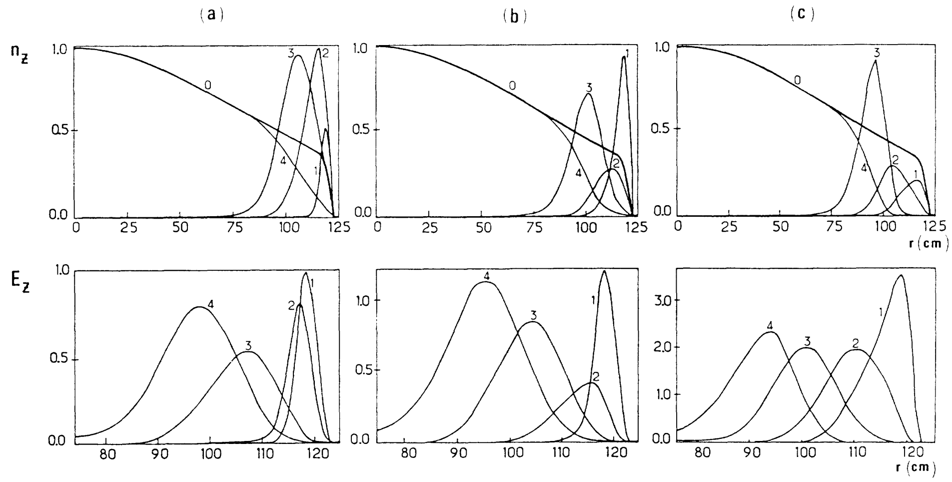

FIG. 8. Simulated ion radial density profiles $n_Z(r)$ (upper) and simulated emissivity radial profiles $E_Z(r)$ (lower): (from left to right) (a) without neutral particles, (b) with $n_D(r)$ from curve 2 of Fig. 7(b), (c) with $n_D(r)$ from curve 3 of Fig. 7(b). Steady-state solution for IW plasmas, $D_A = 10\,000$ cm$^2$/sec, $V_A = 200$ cm/s. Legend of the upper curves including (right) the scale multiplicative factors for cases (a), (b), and (c), respectively. Curve 0: total ion density, 1, 1, 1 scale; curve 1: Li-like ions, 10, 10, 1 scale; curve 2: He-like ions, 5, 1, 1 scale; curve 3: H-like ions, 10, 5, 5 scale; curve 4: fully stripped ions, 1, 1, 1 scale. Legend of the lower curves including (right) the scale multiplicative factors for cases (a), (b), and (c), respectively. Curve 1: C III 977 Å, 1, 1, 1 scale; curve 2: C IV 312.4 Å, 5, 1, 1, scale; curve 3: C V resonance, 10, 5, 5 scale; curve 4: C VI Ly-$\beta$, 100, 50, 50 scale.

varying and less sensitive Ly-$\beta$:Ly-$\delta$ ratio) and on the shape of the simulated spectrum towards the series limit.

For limiter plasmas [the experimental spectrum between 2.5 and 4.2 sec is given in Fig. 3 (upper)] the best correspondence is for curve (2) in Fig. 7(a), suggesting a peripheral $n_D$ density of about $2\times10^9$ cm$^{-3}$, which is very close to the estimated value from $D_\alpha$ emission. Table II shows that for IW plasmas [the experimental spectra between 7.7 and 10 sec and between 13.2 and 14 sec are given in Figs. 4 and 5 (upper) for Ohmic and rf-heated plasmas, respectively], best correspondence is with curve 2 in the case of Ohmic plasmas and with the curve 3 in the case of rf heating. The three chosen simulated spectra are shown in Figs. 3 and 5 (lower).

For the two IW phases studied, the peripheral neutral densities are of the order of $4\times10^{10}$ cm$^{-3}$ and of $4\times10^{11}$ cm$^{-3}$, respectively. These values seem larger than the corresponding values that would be inferred by a quantitative analysis of the $D_\alpha$ monitor signals. With the same assumptions as for the limiter phase, $n_D$ values of about $10^{10}$ cm$^{-3}$ and of a few $10^{10}$ cm$^{-3}$ would be deduced in front of the inner wall for Ohmic and rf-heated plasmas, respectively. Properly the Balmer-$\alpha$ line analysis gives the $n_D$ integrated line density. The situation in IW plasmas is different from that in limiter discharges in the respect that the last closed magnetic surface touches the inner wall. Since the neutral-particle energies and ionization lengths are unknown, reliable quantitative comparison between the two techniques is difficult.

It has to be noted finally that the deduced "experimental" $n_D$ values are actually those existing at the C VI line emitting shells. Figure 8 in conjunction with Table I indicates the distance of these shells from the boundary. From Fig. 7 it appears that at these shells the neutral density is about one order of magnitude less than at the limiter radius and in the SOL.

Finally, we have checked that the emission spectra are essentially unaffected by a variation of either of the two transport parameters ($D_A$ and $V_A$) by up to a factor of 2. Since these variations of the transport parameters can be considered typical for JET Ohmic and rf-heated plasmas,[27,28] it is concluded that $D_A$ and $V_A$ are not sensitive factors as far as the Lyman spectrum is concerned.

TABLE II. Experimental and simulated Ly-$\beta$:Ly-$\gamma$ and Ly-$\beta$:Ly-$\delta$ intensity ratios for the three phases of the discharge studied. The "time" column gives the integration interval of the experimental spectra. Column $C$ indicates the $n_D$ curve number as given in Fig. 7 [(a) for limiter plasmas, (b) for both IW plasmas].

| | Time | Experiment | | Simulation | | | | | | | | |
|---|---|---|---|---|---|---|---|---|---|---|---|---|
| Discharge | (sec) | Ly-$\beta$:Ly-$\gamma$ | Ly-$\beta$:Ly-$\delta$ | $C$ | Ly-$\beta$:Ly-$\gamma$ | Ly-$\beta$:Ly-$\delta$ | $C$ | Ly-$\beta$:Ly-$\gamma$ | Ly-$\beta$:Ly-$\delta$ | $C$ | Ly-$\beta$:Ly-$\gamma$ | Ly-$\beta$:Ly-$\delta$ |
| Limiter | 2.5–4.2 | 2.75 | 6.6 | 1 | 3.0 | 6.7 | 2 | 2.8 | 6.5 | 3 | 2.45 | 6.2 |
| IW | 7.7×10.0 | 1.95 | 4.7 | 1 | 2.15 | 5.9 | 2 | 1.8 | 5.4 | 3 | 1.6 | 5.0 |
| rf-heated IW | 13.2–14.0 | 1.35 | 4.2 | 2 | 1.5 | 4.8 | 3 | 1.35 | 4.5 | 4 | 1.25 | 4.35 |

### D. Qualitative considerations on the carbon ion brightness time evolution

The authenticity of the simulation can, in principle, be checked using absolute line radiances. First, only the C IV and C III absolute line brightnesses are known, as previously mentioned in Sec. II A. But they are not an indication of the volume "average" density of these ions, since the carbon influxes are localized in regions where there is plasma solid material contact.[10] An estimation of the carbon content (carbon is the man impurity in the discharge studied) could be given by the $Z_{\text{eff}}$ values from visible bremsstrahlung emission. Its value is nearly constant at about 3. However, the presence of a few percent of $^3$He (which is not measurable precisely in the discharge) prevents any accurate quantitative inference based on $Z_{\text{eff}}$.

Qualitatively, our analysis shows it is impossible to simulate the constancy of C VI Ly-$\alpha$ and Ly-$\beta$ and of C V resonance lines at the limiter–inner-wall transition without modifying the transport parameters. This is a consequence as of the dependence of the C ion brightnesses on the neutral density $n_{\text{D}}$ discussed in Sec. IV B. Physically an increase of the peaking of the carbon ion total density profile (i.e., of the $V_A/D_A$ ratio) after moving to the inner wall would require less peripheral carbon ions to generate the same central carbon ion density. Such a reduction would compensate for the increase in brightnesses, that would otherwise result from the increased $n_{\text{D}}$ dependence of brightnesses.

The relative constancy of Ly-$\alpha$ with respect to Ly-$\beta$ is correctly simulated, since their ratio is always found of the order of 8.5–9. The relative variations of Balmer $\alpha$ with respect to Lyman $\alpha$ are in agreement with their relative time evolutions shown in Fig. 2. The three "spectral best fitting" simulations give brightness ratios equal to 0.07, 0.12, and 0.17, respectively, on taking $F(n)=1$ for both lines.

Experimental values for the $G$ ratio, with the hole correction included, are found to be equal to 0.45–0.50 for limiter plasmas and to 0.65–0.7 for both IW plasmas. Again for the three spectral best fitting conditions, we find, respectively, 0.49, 0.74, and 0.77. We consider the agreement quite satisfactory, bearing in mind the experimental uncertainties, the inaccuracies of the atomic physics model, and the fact that the $G$ ratio is an inverse function of $T_e$ and therefore quite sensitive to errors in the peripheral $T_e$ profile. It has, however, to be stressed that to simulate $G$ ratios larger than 0.60 in plasma regions with $T_e$ larger than about 150–200 eV requires the charge-exchange population of the triplet levels to be taken into account.

## V. CONCLUSIONS

In hot JET deuterium plasmas, C VI emission arises from collision processes, which, in the absence of neutral hydrogen beam heating, occur near the plasma boundary. In comparison with the limiter discharges, distortions to the Lyman decrement (such as Ly-$\beta$:Ly-$\gamma$ and Ly-$\beta$:Ly-$\delta$ ratios) and enhancements of the high-series members (around 1$s$-12$p$) are observed after the plasma has been brought into contact with the carbon inner wall.

The intensities of the Lyman spectrum members are interpreted in terms of low-energy electron transfer from thermal $\text{D}^0$ atoms to $\text{C}^{6+}$ ions as well as electron excitation of $\text{C}^{5+}$ in their ground state.

The line-of-sight emission along the major torus radius is modeled using an impurity transport code which uses the experimental $n_e$ and $T_e$ radial profiles. The neutral deuterium density profile is introduced into the code by maintaining the central region values in the range given by NPA data analysis, while the peripheral values towards the limiter radius are adjusted to match the experimental results.

Electron transfer from excited states of $\text{D}^0$ (up to $n=5$) as well as from the ground state have to be included to give satisfactory agreement with the Lyman spectra for Ohmic and rf-heated plasmas. The cross sections for charge exchange from the ground state are obtained from the CCMO model,[23] whereas those for charge exchange from excited states have been estimated using a simple universal Landzu-Zener model. Comparisons of relative intensities with model calculations allow plausible corrections $F(n)$ to be made to the effective charge-exchange rate coefficients $Q_{n-1}^{\text{CE}}$ as a function of the principal quantum number $n$ of the upper level. For large-$n$ values, $F(n)$ is determined in such a way as to reproduce the experimental spectrum towards the series limit (including the observed bump around $n=12$), whereas for $n=4,5$ $F(n)$ is chosen in such a way as to simulate the Ly-$\beta$:Ly-$\gamma$ and the Ly-$\beta$:Ly-$\delta$ ratios. Taking $F(4,5)=1$, it was not possible to simulate the smallest ratios observed experimentally [even on increasing $n_{\text{D}}(r)$ up to a maximum reasonable limit based on NPA and $\text{D}_\alpha$ monitor data]. These low-$n$ $F(n)$ values must also not be too large, to maintain consistency with the total charge-exchange cross section, which is believed to be quite reliable. Moreover, for limiter plasmas, with well-defined scrape-off layers, the modeling of $\text{D}_\alpha$ monitor signals gives plausible values for the peripheral $\text{D}^0$ densities [$\sim(1.5-3)\times10^9$ cm$^{-3}$] which are also correctly obtained by the Lyman spectrum simulations. On the other hand, for Ohmic inner-wall and rf-heated inner-wall plasmas the necessary peripheral $\text{D}^0$ densities for the simulations are one and two orders of magnitude higher, respectively. Comparison with the $\text{D}_\alpha$ signals from the inner wall is prevented by the unknown $\text{D}^0$ ionization length in front of the inner wall.

The analyzed data refer to the region $r/a_L\sim0.8$, where the Lyman-series emission shells are located. In this region the $n_{\text{D}}$ values are approximately one order of magnitude less than at the true periphery.

The observations offer a potential method of measuring local $\text{D}^0$ concentrations near the boundary of high-temperature, high-$\text{D}^0$ recycling plasmas. The method relies upon good peripheral $n_e(r)$ and $T_e(r)$ profiles around $r/a_L\sim0.7-0.9$ and reliable extrapolation into the scrape-off layer. The present accuracy of this method of determining $n_{\text{D}}(r)$ curves from spectral features is to within an order of magnitude at the plasma boundary.

This is the difference between the peripheral values of the $n_D(r)$ curves shown in Fig. 7 and used for the numerical simulations.

Difficulties were found in simulating the correct brightness time evolutions at the limiter to inner-wall shift. This is especially true for the almost constant intensity of the C VI and C V resonance lines. Results are inconclusive, but they do imply necessarily a change of the impurity total density profile, which must be more peaked for IW plasmas. On the other hand, the relative variations of both the C VI Ly-$\beta$ and Balmer-$\alpha$ lines relative to the C VI Ly-$\alpha$ line and the increased $G$ ratios after moving to inner wall were satisfactorily simulated. For the latter the inclusion of charge-exchange recombination into the triplet levels is essential. Simulations of the less ionized species C IV and C III lines were not attempted, since their emission is localized in front of the inner wall.[10]

Unfortunately, we cannot avoid the criticism of using a one-dimensional transport code for simulating IW plasmas, when the xuv spectrometer is looking directly at the source of neutral particles. The deuterium visible light monitors and the long-wavelength survey spectrometer confirm poloidal asymmetries when the plasma is moved in the inner wall. There is every reason to expect that the neutral deuterium distribution can only be accurately described with a full three-dimensional neutral-particle transport model for these plasmas conditions. For limiter plasmas, C VI emission is certainly poloidally symmetric, since the radial profiles of the O VI 1032-Å line have always been found as expected for a poloidal symmetric shell.[30] Due to the spreading of the impurity ions along the field lines the asymmetries are progressively reduced as the ionization potentials of the ions increase, and C VI has an ionization potential much larger than O VI. The quantitative analysis reported in Ref. 10 indicates that O VI emission should approach poloidal symmetry in IW plasmas and, consequently, there is good reason to believe that C VI emission is poloidally symmetric. Also the deuterium atom distribution at about 1 m from the plasma center should approach this condition of poloidal symmetry, but this still has to be verified.

The $F(n)$ corrections for $n=4,5$ are of the order of the expected accuracy of the cross-section evaluations for charge-exchange from ground-state $D^0$ atoms. By contrast, $F(n)$ corrections for higher $n$ are fairly large. The simple universal Landau-Zener model adopted as a starting point for the present study has no prior demonstration of reliability for capture from excited $D^0$ states. The general expectation is that it should give a lower limit for results and this appears to be confirmed here. Detailed studies in progress show that indeed the charge exchange from excited states of deuterium at low energy is dominated by a small number of active curve crossings and that a Landau-Zener approximation is a suitable starting point. However, the accurate Landau-Zener parameters are significantly different from those adopted here. Also the crossing radii, corresponding to a given initial $D^0$ $n$ shell, vary significantly for the different molecular symmetries. It is anticipated that the more accurate calculations to be published will confirm the trend of multipliers $F(n)$ indicated by the experiment here.

The region of $n \geq 15$ up to the series limit cannot be considered adequately treated in the present work. The analysis procedure has exploited the separability of excitation and charge-exchange parts of the effective rate coefficients for photon emission. Also the deuterium collision limit has been introduced sharply into the calculations. In the continuation through the $C^{5+}$ collision limit to the series limit and on into the free-bound continuum, clearly radiative recombination, three-body recombination and collisional-radiative processes between $n$ shells should enter the calculations. These refinements should not disturb the present conclusions covering the region $n \leq 15$.

## ACKNOWLEDGMENTS

We would like to acknowledge the JET team for making this study possible, for technical support, and for providing other diagnostic information. In particular, it is a pleasure to acknowledge discussions with Dr. S. Corti and Dr. P. Morgan and their permission to use experimental data from the neutral-particle analyzers and from the $D_\alpha$ monitors. Thanks are due also to Dr. B. Saoutic who developed the extension of the impurity-ion transport code to large plasma sizes.

---

[1] R. C. Isler, Phys. Scr. **35**, 650 (1987).

[2] A. Boileau, M. Von Hellermann, L. D. Horton, J. Spence, and H. P. Summers, Plasma Phys. Contr. Fusion **31**, 779 (1989).

[3] J. E. Rice, E. S. Marmar, J. L. Terry, E. Källne, and J. Källne, Phys. Rev. Lett. **56**, 50 (1986).

[4] J. E. Rice, E. S. Marmar, E. Källne, and J. Källne, Phys. Rev. A **35**, 3033 (1987).

[5] R. C. Isler and R. E. Olson, Phys. Rev. A **37**, 3399 (1988).

[6] J. L. Schwob, A. W. Wouters, S. Suckewer, and M. Finkenthal, Rev. Sci. Instrum. **58**, 1601 (1987).

[7] R. J. Fonck, A. T. Ramsey, and R. V. Yelle, Appl. Opt. **21**, 2115 (1982).

[8] H. Salzmann, K. Hirsch, P. Nielsen, C. Gowers, A. Godd, M. Gadeberg, H. Murmann, and C. Schrödter, Nucl. Fusion **27**, 1925 (1987).

[9] D. Veron, in *Workshop on Diagnostics for Fusion Reactor Conditions, Varenna, 1982,* edited by P. E. Stott, D. K. Akulina, G. G. Leotta, E. Sindoni, and C. Wharton (Commission of European Communities, Brussels, 1983), p. 283.

[10] K. H. Behringer, B. Denne, M. J. Forrest, M. F. Stamp, and H. P. Summers, JET Report No. JET-P(85)31, 1985 (unpublished).

[11] B. Saoutic, J. Ramette, M. Mattioli, B. Denne, K. Behringer, G. Magyar, N. Peacock, A. Ravestein, J. L. Schwob, F. Sieweke, and A. Talbot, JET Report No. JET-R(87)14, 1987 (unpublished).

[12] K. Behringer, B. Denne, G. Magyar, M. Mattioli, N. J. Peacock, J. Ramette, B. Saoutic, and J. L.Schwob, J. Phys. (Paris), Colloq. Suppl. 3, **49**, C1-387 (1988).

[13] J. G. Timothy, Rev. Sci. Instrum. **52**, 1131 (1981).

[14] TFR Group, Nucl. Fusion **25**, 981 (1985).

[15] K. Lackner, K. Behringer, W. Engelhardt, and R. Wunder-

lich, Z. Naturforsch. **37a**, 931 (1982).

[16]K. L. Bell, H. B. Gilbody, J. G. Hughes, A. E. Kingston, and F. J. Smith, J. Phys. Chem. Ref. Data **12**, 891 (1983).

[17]M. A. Lennon, K. L. Bell, H. B. Gilbody, J. G. Hughes, A. E. Kingston, M. J. Murray, and F. J. Smith, J. Phys. Chem. Ref. Data **17**, 1285 (1988).

[18]M. Mattioli, Cadarache Laboratory Report No. EUR-CEA-FC 1346, 1988 (unpublished).

[19]R. A. Phaneuf, R. K. Janev, and M. S. Pindzola (editors) ORNL Report No. ORNL-6090/V5 (1987).

[20]M. Mattioli, N. J. Peacock, H. P. Summers, B. Denne and N. C. Hawkes, JET Report No. JET-P(89)06, 1989 (unpublished).

[21]TFR Group, J. G. Doyle, and J. L. Schwob, J. Phys. B **15**, 813 (1982).

[22]J. Spence and H. P. Summers, J. Phys. B **19**, 3749 (1986).

[23]T. A. Green, E. J.Shipsey, and J. C. Browne, Phys. Rev. A **25**, 1364 (1982).

[24]R. E. Olson and A. Salop, Phys. Rev. A **14**, 579 (1976).

[25]R. Mann, F. Folkmann, and H. F. Beyer, J. Phys. B **14**, 1161 (1981).

[26]S. Corti, G. Bracco, M. Brusati, A. Gondhalekar, G. Grosso, F. Hendriks, S. Segre, and V. Zanza, in *Twelfth European Conference on Controlled Fusion and Plasma Physics, Budapest, 1985,* edited by L. Pocs and A. Montvai (European Physical Society, Geneva, 1985), Vol. I, p. 219.

[27]K. H. Behringer, P. G. Carolan, B. Denne, G. Decker, W. Engelhardt, M. J. Forrest, R. Gill, N. Gottardi, N. C. Hawkes, E. Källne, H. Krause, G. Magyar, M. Mansfield, F. Mast, P. Morgan, N. J. Peacock, M. F. Stamp, and H. P. Summers, Nucl. Fusion **26**, 751 (1986).

[28]K. Behringer, A. Boileau, F. Bombarda, G. B. Denne, W. Engelhardt, M. J. Forrest, G. Fussmann, R. Giannella, N. A. Gottardi, M. Von Hellermann, L. Horton, H. Jäckel, C. Jupén, E. Källne, K. D. Lawson, G. Magyar, G. M. McCracken, P. D. Morgan, E. R. Müller, N. J. Peacock, J. Ramette, B. Saoutic, M. F. Stamp, H. P. Summers, G. Tallents, and A. Weller, in *Plasma Physics and Controlled Nuclear Fusion Research,* Proceedings of the Eleventh Conference, Kyoto, 1986, (IAEA, Vienna, 1987), Vol. 1, p. 197.

[29]L. C. Johnson and E. Hinnov, J. Quant. Spectrosc. Radiat. Transfer **13**, 333 (1973).

[30]K. H. Behringer, C. Breton, C. de Michelis, B. Denne, G. Magyar, J. Ramette, and B. Saoutic, in *Basic and Advanced Diagnostic Techniques for Fusion Plasmas, Varenna, 1987,* edited by P. E. Stott, D. K. Akulina, G. G. Leotta, E. Sindomi, and C. Wharton (Commission of the European Communities, Brussells, 1987), Vol. I, p. 305.